Static and Dynamic Studies for Coupling Discrete and Continuum Media; Application to a Simple Railway Track Model

Mohammad Hammoud, Denis Duhamel, Karam Sab

▶ **To cite this version:**

Mohammad Hammoud, Denis Duhamel, Karam Sab. Static and Dynamic Studies for Coupling Discrete and Continuum Media; Application to a Simple Railway Track Model. International Journal of Solids and Structures, 2010, 47 (2), pp.276-290. ⟨10.1016/j.ijsolstr.2009.09.036⟩. ⟨hal-00517323⟩

HAL Id: hal-00517323

https://hal.science/hal-00517323v1

Submitted on 14 Sep 2010

HAL is a multi-disciplinary open access archive for the deposit and dissemination of scientific research documents, whether they are published or not. The documents may come from teaching and research institutions in France or abroad, or from public or private research centers.

L'archive ouverte pluridisciplinaire **HAL**, est destinée au dépôt et à la diffusion de documents scientifiques de niveau recherche, publiés ou non, émanant des établissements d'enseignement et de recherche français ou étrangers, des laboratoires publics ou privés.

HAL Authorization

Static and Dynamic Studies for Coupling Discrete and Continuum Media; Application to a Simple Railway Track Model

Mohammad Hammoud[a,*], Denis Duhamel[a], Karam Sab[a]

[a] *Université Paris-Est, UR Navier, Ecole des Ponts ParisTech, 6 et 8 Avenue Blaise Pascal, Cité Descartes, Champs sur Marne, 77455 Marne La Vallée, Cedex 2, France*

Abstract

In this paper, we present a formulation for coupling discrete and continuum models for both dynamic and static analyses. This kind of formulation offers the possibility of carrying out better simulations of material properties than the discrete calculations, and with both larger length scales and longer times. Using only a discrete approach to simulate a large medium composed of many degrees of freedom seems very difficult in terms of calculation and implementation. Moreover, using only a continuum approach does not give an accurate solution in a zone where particular and localized phenomena can occur. A direct application of our coupling approach to the case of railway track models subjected to an external load, is proposed for its validation.

Key words: Discrete model, Continuum model, Static, Dynamic, Coupling, Multiscale.

*Corresponding Author. Tel: +33 1 64 15 37 36, Fax: +33 1 64 15 37 41.
Email addresses: hammoudm@lami.enpc.fr (Mohammad Hammoud)

1. Introduction

The main objective of the modeling of modern materials is to predict the response and failure of materials which are governed by deformation mechanisms. For many material simulations, it is very difficult to make a discrete calculation because of large Representative Volume Element sizes and important computation times. Moreover, using only a continuum approach does not always provide an accurate simulation for the response of the system being studied. These two main problems forced researchers to reconsider the advantages of each approach and to recognize that a coupling methodology had to be established that would combine the advantages of both discrete and continuum modelings. Although this field has been studied in the past, it still remains an active area of research (see (Kohlhoff et al, 1989), (Shenoy et al, 1999), (Frangin et al, 2006), (Klein et al, 2006), (Cundall et al, 1979), (Tadmor et al, 1996), (Broughton et al, 1999) and (Miller & Tadmor, 2009)). In our study, we are interested in using a coupling method applicable to a simple model for high-speed train tracks consisting in a beam resting on very large number of springs (see Figure 1).

Figure 1 is approximately here

Existing coupling methodologies can be classified as:
Bottom-up methods, Top-down Methods, and Direct Methods.
The idea of the Bottom-up methods is to solve the non-linear equations at the macroscopic scale by the extraction of the behavior laws from an atomic description at the microscopic scale.

Tadmor et al (1996) developed the Quasicontinuum method (**QC**). The QC uses Finite Elements (FE) representation of the displacement field over the entire domain, requiring mesh refinement to the atomic scale in regions of severe deformation. The strain energy within the element is determined from a single "**representative atom**" embedded in a locally constructed crystallite. Consistency between refined and coarse areas is achieved by using the finite deformation elasticity and the Cauchy-Born rule that equates interatomic bond energy to continuum potential energy in order to develop a non-linear continuum constitutive model based on the interatomic potential used for atomistic simulations. While the QC approach allows a blending between atomistic and continuum regions, it has the disadvantages of relying on an adaptive mesh refinement to the atomic scale, a computationally intensive task, and an inability to eliminate fictitious boundary effects at the local/non-local boundary.
The bridging Scale Decomposition (**BSD**) approach was first used by Wagner & Liu (2003). The starting point of the method involves the use of a bridging subdomain in which the Hamiltonian is chosen as a linear combination of discrete and continuum Hamiltonians. In the bridging domain, Discrete Element (DE) degrees of freedom and Finite Element (FE) ones are linked by Lagrange multipliers. Numerical methods are employed to solve the problem of spurious wave reflections which appear at the interface due to the size of the discontinuities of the discretization. The (**BSD**) is more developed by Xiao & Belytschko (2004) and later Frangin Frangin et al (2006). In the bridging domain, the compatibility is enforced by Lagrange multipliers or by an augmented Lagrangian method.

The idea of the Top-down method is to treat the atoms per unit cell as "coarse grains" and to construct the associated energy which converges to the exact atomic energy in order to derive the atomic equations. A brief description of some of these methods follows.

Rudd & Broughton (1998) developed the Coarse-Grained Molecular Dynamic method (**CGMD**) which consists of replacing the underlying atomic lattice with nodes representing either individual atoms or a weighted average of a collection of atoms. The total energy of the system is calculated from the potential and kinetic energies of the nodes in addition to a thermal energy term representing the missing degrees of freedom assumed to be at a uniform temperature.

Broughton et al (1999) introduced the Molecular Atomistic Ab-initio Dynamic (**MAAD**) approach. The MAAD approach separates the physical system into distinct MD and FE regions. The total Hamiltonian of the system consists of contributions from each individual region as well as a contribution from the **hand shaking** (Bridging domain) between regions. The FE mesh in this hand-shaking zone is refined to the atomic scale and the nodes occupy the positions where the atoms would be if the atomic region were extended into the FE domain. Kinetic energy is attributed to both nodes and atoms in the hand-shaking zone, while further from this zone, uniform temperature terms are added to account for the missing degrees of freedom. This approach has successfully performed non-reflective transmissions of elastic waves between MD and FE regions.

The Direct Methods consist of the decomposition of a spatial domain into subdomains; a continuum domain, an atomic domain and finally a

hand-shake domain.
(Ben Dhia & Rateau, 2001) and (Ben Dhia & Rateau, 2005) introduced the Arlequin method as a flexible engineering design tool. This method is able to introduce local defects (such as cracks, holes or inclusions) with great flexibility in a global existing coarse model. Also this method is able to change the local behavior in a globally simplified model of a given material.

Figure 2 is approximately here

In the Arlequin method the total energy of the system is formulated as follows:

$$E_{\text{system}} = E^{(\Omega_1 \setminus \Omega_2)}(u_1) + E^{(\Omega_2 \setminus \Omega_1)}(u_2) + \alpha_1 E^{(\Omega_s)}(u_1) + \alpha_2 E^{(\Omega_s)}(u_2)$$

$E^{(\Omega_1 \setminus \Omega_2)}(u_1)$ and $E^{(\Omega_2 \setminus \Omega_1)}(u_2)$ are the potential energy of the field solutions (u_1) and (u_2) in the domains Ω_1 and Ω_2 without the intersection domain Ω_s, respectively. $E^{(\Omega_s)}(u_1)$ and $E^{(\Omega_s)}(u_2)$ are the potential energy of the intersection domain of the field solutions (u_1) and (u_2), respectively.

In the above paragraphs we presented the coupling methods successfully employed to simulate material deformations such as crack-grain boundary interactions, dislocation nucleations from nanoindentation and the dynamic fracture of silicon. However, the weaknesses of these methods shows that more work is needed to develop a coupling atomistic-continuum approach. As already mentioned, the improper partitioning of the system's potential energy leads to the appearance of nonexistant forces acting on atoms and nodes within the overlap region. These forces are often referred to as

"**ghost forces**" and are often the continued development of atomistic/continuum coupling methods. For instance, the recent review article by (Curtin & Miller (2003) and Miller & Tadmor (2009)) describes the origins and effects of the ghost forces that arise from using the QC method. They are also revised in an approach by Shenoy et al (1999) to determine corrections that can be introduced to the QC methodology to compensate for ghost forces. This approach involves the use of dead loads equal and opposite to the ghost forces determined from the undeformed configuration of the system. While the introduction of this correction is noteworthy, it inevitably leads to inaccuracies once the crystal becomes deformed, even for homogeneous loading conditions, or if the lattice is subjected to any rotation. Also, Curtin discuss the developpement by Knap et al (2001) of a fully non-local formulation of the QC method. This approach avoids using the Cauchy/Born rule and instead determines nodal forces by constructing a small cluster of representative atoms surrounding a node and calculating the force using the non-local, atomistic description.
In all the approaches presented above, it is evident that the issue of how to partition energy within atomistic-continuum overlap regions needs to be addressed properly in order to maintain the integrity of the two views of material deformation, discrete and continuum, and to obtain accurate solutions.
In our proposed coupling approach, due to the reasons mentioned earlier, the mechanical parameters of the system being studied will be calculated in an indirect way that does not require the calculation of the energy and avoids the problem of how to partition this energy between the discrete and

continuum zones.

In this paper, after this introduction of the coupling existing methodologies, we present a 1D railway track model (see Ricci et al (2005), Nguyen & Duhamel (2006), Nguyen & Duhamel (2008) and Al Shaer et al (2008), Bodin-Bourgoin et al (2006)). This model consists of a beam resting on many elastic springs. The deflection of the beam (as well as the nodal parameters) is calculated with two approaches; a discrete approach and a macroscopic approach deduced from the discrete one. First, a comparison between the responses of the system obtained by using these two approaches is made in order to determine the cases where the macroscopic approach cannot replace the discrete one. Then, we apply a Discrete/Continuum coupling method to these cases. Finally, numerical results are presented in order to validate and prove the efficiency of the proposed coupling method.

2. Discrete and Continuum formulations

2.1. Discrete approach

A beam resting on springs and on which we apply a load F is shown in Figure 1. It represents a railway under which the track tie and the ballast layer are modeled by elastic springs as the supports of the beam. Firstly, the applied load is assumed to be fixed, so in this case a static problem is studied.

2.1.1. Static solution

The static equilibrium equation of the discrete approach is written as follows:

$$EIu^{(4)}(x) + \sum_{i=1}^{N} h\, k_i u(x_i)\delta\,(x - x_i) = F\delta(x - D) \tag{1}$$

In Figure 1, L and x_i are the total length of the beam and the positions of the springs along the beam (with $x = 0$ being the left endpoint of the beam) respectively. In Equation (1) D, h and k_i are the distance of the loading force from the left end of the beam, the spacing between consecutive track ties, and the stiffness of the springs respectively. N represents the number of track ties.

Figure 3 is approximately here

First, let us consider two adjacent elements of the beam (see Figure 3). A concentrated force F acts vertically on one of the elements at a distance Y from the left-hand end point of the element. Then we seek to calculate the deflection which minimizes the total microscopic energy of the beam, the springs, and the load.

First a relationship between any two consecutive vectors of parameters must be established. A vector of parameters consists of the vector which contains the parameters of each node; the deflection, rotation, bending moment, and shear force.

Formulation of the parameters and of the stiffness matrix

In this paragraph, we are interested in solving the 4^{th} order differential Equation (1) analytically. The third derivative of the deflection $u(x)$ is not continuous on the segment $[0, h_1]$ on which the load F is applied. It is discontinuous before and after the crossing point between the two segments.

Consequently :

$$\begin{cases} u'''(x) = A \quad \text{on} \quad [0, Y^-] \\ u'''(x) = P \quad \text{on} \quad [Y^+, h_1] \end{cases} \tag{2}$$

Where A and P are two constants. By applying 3 times the integral operation on $u'''(x) = A$ and $u'''(x) = P$, this gives us a system of two equations containing 8 variables. This system is formulated as follows:

$$u(x) = A\frac{x^3}{6} + B\frac{x^2}{2} + Cx + D \quad \text{on } [0, Y^-] \tag{3}$$

$$u(x) = P\frac{(x-h_1)^3}{6} + Q\frac{(x-h_1)^2}{2} + R(x-h_1) + S \quad \text{on } [Y^+, h_1] \tag{4}$$

To find the eight unknown coefficients which exist in Equations (3) and (4), we suppose that u, $u^{'}$, $u^{''}$ and $u^{'''}$ have known values at the node 0, so $u^{'''}(0) = A$, $u^{''}(0) = B$, $u^{''}(0) = C$ and $u(0) = D$. To these boundary conditions is added the conditions of continuity at the point of load "Y" on u, $u^{'}$, $u^{''}$ and a jump condition on $u^{'''}$. These conditions of continuities are formulated in the system of Equation (5).

$$\begin{cases} u\left(Y^+\right) = u\left(Y^-\right) \\ u^{'}\left(Y^+\right) = u^{'}\left(Y^-\right) \\ u^{''}\left(Y^+\right) = u^{''}\left(Y^-\right) \\ P - A = \dfrac{F}{EI} \end{cases} \tag{5}$$

Finally, these conditions added to the relations between different vectors of parameters (see Appendix), lead us to the following values of P, Q, R and S.

$$
\begin{aligned}
S = u(h) &= u(0) + hu^{'}(0) + \frac{h^2}{2EI}u^{''}(0) + \frac{h^3}{6EI}u^{'''}(0) - F\frac{(Y-h)^3}{6EI} \\
R = u^{'}(h) &= u^{'}(0) + hu^{''}(0) + \frac{h^2}{2EI}u^{'''}(0) + F\frac{(Y-h)^2}{2EI} \\
Q = u^{''}(h) &= u^{''}(0) + hu^{'''}(0) - F\frac{(Y-h)}{EI} \\
P = u^{'''}(h) &= u^{'''}(0) + \frac{F}{EI}
\end{aligned} \tag{6}
$$

A jump condition between two consecutive beam elements created by the spring of stiffness k is given by Equation (7). It will be used later in the stiffness matrix.

$$
u^{'''}(h_1{}^{-}) - u^{'''}(h_1{}^{+}) = \frac{k}{EI}u(h_1{}^{-}) \tag{7}
$$

Indeed $u(0)$, $u'(0)$, $(-EI\,u''(0))$ and $(-EI\,u'''(0))$ represent the deflection u_0, the rotation θ_0, the bending moment M_0 and the shear force T_0 respectively.

By using the Equations (3) and (4) that give the form of the deflection u and by considering the jump condition in Equation (7), a relationship between the vector of force $\mathbf{F_{01}} = [T_0\ M_0\ T_1\ M_1]^T$ and the vector of displacement $\mathbf{U_{01}} = [u_0\ \theta_0\ u_1\ \theta_1]^T$ in the element can be formulated as follows:

$$
\mathbf{F_{01}} = \mathbf{K}_{01}\,\mathbf{U_{01}} + \mathbf{R} \tag{8}
$$

Where the matrix $\mathbf{K_{01}}$ and the vector of $\mathbf{R}$ are written as follows:

$$\mathbf{K}_{01} = EI \begin{bmatrix} \frac{12}{h^3} & \frac{6}{h^2} & -\frac{12}{h^3} & \frac{6}{h^2} \\ \frac{6}{h^2} & \frac{4}{h} & -\frac{6}{h^2} & \frac{2}{h} \\ -\frac{12}{h^3} & -\frac{6}{h^2} & \frac{12}{h^3} - \frac{k_1}{EI} & -\frac{6}{h^2} \\ \frac{6}{h^2} & \frac{2}{h} & -\frac{6}{h^2} & \frac{4}{h} \end{bmatrix} \; ; \; \mathbf{R} = F \begin{bmatrix} \frac{-2\,Y^3 + 3Y^2\,h - h^3}{h^3} \\ \frac{-Y^3 + 2\,Y^2\,h - Y\,h^2}{h^2} \\ \frac{2\,Y^3 - 3Y^2\,h}{h^3} \\ \frac{-Y^3 + Y^2\,h}{h^2} \end{bmatrix} \tag{9}$$

$\mathbf{K_{01}}$ is the stiffness matrix. It depends only on the stiffness of spring "k_1" and the spacing between two consecutive springs "h". If the external load is applied within the segment, we assume the existence of the vector $\mathbf{R}$ associated with the applied load F.

We can simplify Equation (8) to a beam resting on N springs by considering that the elements of the connection matrix depend only on k_i and h.

$$\begin{cases} \mathbf{F_{i\,i+1}} = \mathbf{K}_{i\,i+1}\,\mathbf{U_{i\,i+1}} + \mathbf{R} & \text{load is applied within the segment} \\ \mathbf{F_{i\,i+1}} = \mathbf{K}_{i\,i+1}\,\mathbf{U_{i\,i+1}} & \text{otherwise} \end{cases} \tag{10}$$

2.1.2. Dynamic solution

In this section, a simplified dynamic study is considered. The applied load is harmonic and we are interested in the harmonic dynamic response as the real part of $u(x)\,e^{i\omega\,t}$. So the dynamic equilibrium equation is formulated as follows:

$$EI\,u^{(4)}(x) + \sum_{i=1}^{N} h\,k_i u(x_i)\delta\,(x - x_i) - \rho\omega^2 S u(x) = F\delta(x - D) \tag{11}$$

ρ, S, ω are the density of the steel, the section of the rail and the angular frequency of the wave exciting the beam, respectively.

The characteristic polynomial of the differential equation (11), where the solution takes an exponential form $e^{\xi x}$, is:

$$\xi^4 - \frac{\rho\omega^2 S}{E\,I} = 0 \tag{12}$$

Equation (12) possesses four complex roots; $\xi_j = r_j + iq_j$ where r_j and q_j represent the attenuation and the propagation part of the wave respectively. The semi analytical solution of the differential Equation (11) takes the following exponential form:

$$u(x) = \alpha\, e^{\xi x} + \beta\, e^{-\xi x} + \gamma\, e^{i\xi x} + \delta\, e^{-i\xi x} \tag{13}$$

Where α, β, γ and δ are constants that must be calculated at each element in order to find the deflection of the discrete approach in the dynamic case. Let us consider two adjacent elements of the beam (see Figure 4).

Figure 4 is approximately here

As in the static case we have to consider two cases:

• First case: the load is applied within the beam at the point of load "Y" (see Figure 4). The three conditions of continuities on $u(x)$, $u'(x)$ and $u''(x)$ and the jump condition on $u'''(x)$ are the same as those in Equation (5).
A relationship between the vectors g and U_0 can be established. U_0 consists of the vector of deflection $u(0)$, rotation $u'(0)$, bending moment $(-EI\,u_0'')$ and shear force $(-EI\,u_0''')$ at the first node and $g = [\alpha\ \beta\ \gamma\ \delta]$.
The relationship between g and U_0 is deduced from the solution of the

diffrential Equation (13) and formulated in matrix form in Equation (14):

$$U_0 = \begin{bmatrix} u_0 \\ \theta_0 \\ M_0 \\ T_0 \end{bmatrix} = \begin{bmatrix} 1 & 1 & 1 & 1 \\ \xi_0 & -\xi_0 & i\,\xi_0 & -i\,\xi_0 \\ -E\,I\,\xi_0^2 & -E\,I\,\xi_0^2 & E\,I\,\xi_0^2 & E\,I\,\xi_0^2 \\ -E\,I\,\xi_0^3 & E\,I\,\xi_0^3 & i\,E\,I\,\xi_0^3 & -i\,E\,I\,\xi_0^3 \end{bmatrix} \begin{bmatrix} \alpha \\ \beta \\ \gamma \\ \delta \end{bmatrix} = R_1\, g \tag{14}$$

Similarly, a relationship between the vectors $\tilde{g} = [\tilde{\alpha}\ \tilde{\beta}\ \tilde{\gamma}\ \tilde{\delta}]$ and U_h is established. It is written in the following matrix form:

$$U_h = \begin{bmatrix} u_h \\ \theta_h \\ M_h \\ T_h \end{bmatrix} = \begin{bmatrix} a_0 & b_0 & c_0 & d_0 \\ \xi_0\,a_0 & -\xi_0\,b_0 & i\,\xi_0\,c_0 & -i\,\xi_0\,d_0 \\ -E\,I\,\xi_0^2\,a_0 & -E\,I\,\xi_0^2\,b_0 & E\,I\,\xi_0^2\,c_0 & E\,I\,\xi_0^2\,d_0 \\ -E\,I\,\xi_0^3\,a_0 & E\,I\,\xi_0^3\,b_0 & i\,E\,I\,\xi_0^3\,c_0 & -i\,E\,I\,\xi_0^3\,d_0 \end{bmatrix} \begin{bmatrix} \tilde{\alpha} \\ \tilde{\beta} \\ \tilde{\gamma} \\ \tilde{\delta} \end{bmatrix} = R_4\, \tilde{g} \tag{15}$$

Where $a_0 = e^{\xi_0 L_1}$, $b_0 = e^{-\xi_0 L_1}$, $c_0 = e^{i\,\xi_0 L_1}$ and $d_0 = e^{-i\,\xi_0 L_1}$.

The matrix R_4 is calculated using the general solution of the differential Equation (13) $u(x)$ and its derivative $u'(x)$, $u''(x)$ and $u'''(x)$ at the node L_1^-.

Using the equalities in Equations (5), (14), and (15), the following relationship between U_0 and U_h is found:

$$U_h = R_4\, {R_3}^{-1}\, R_2\, {R_1}^{-1}\, U_0 + R_4\, {R_3}^{-1}\, \frac{F}{EI} \tag{16}$$

Where R_1 and R_4 are the matrices calculated in Equations (14) and (15), R_2 and R_3 are the matrices calculated in the appendix (see Equation (44)). In here $R_2 = R_3$, thus Equation (16) is simplified as:

$$U_h = R_4\ {R_1}^{-1}\, U_0 + R_4\, {R_3}^{-1}\, \frac{F}{EI}$$

• Second case: The load is applied outside the first element

In this case, only Equations (14) and (15) are used to link the vector U_h to U_0. This relationship is written as follows:

$$U_h = R_4 \, {R_1}^{-1} \, U_0 \tag{17}$$

Finally, we generalize the relations in Equations (16) and (17) for a beam resting on N springs as follows:

$$\begin{cases} \mathbf{U_{i+1}} = R_4 \, {R_1}^{-1} \, \mathbf{U_i} + R_4 \, R_3^{-1} \, \dfrac{F}{EI} & \text{load within the beam} \\ \mathbf{U_{i+1}} = R_4 \, {R_1}^{-1} \, \mathbf{U_i} & \text{otherwise} \end{cases} \tag{18}$$

The relationship between the vector of force $\mathbf{F_{i\,i+1}} = [T_i \; M_i \; T_{i+1} \; M_{i+1}]^T$ and the vector of displacement $\mathbf{U_{i\,i+1}} = [u_i \; \theta_i \; u_{i+1} \; \theta_{i+1}]^T$ is calculated using numerical methods during the simulation in MATLAB code.

2.2. Macroscopic approach

A macroscopic approach is deduced from the discrete one at the macroscopic scale. In this approach, we proceed by the homogenization of the beam relative to the stiffnesses of the springs (Fig 5). In the microscopic approach we start with an enormous number of degrees of freedom (DoF), whereas homogenisation is used to replace the zones that have homogeneous DoF with only one DoF, which will then reduce the required computing time.

Figure 5 is approximately here

2.2.1. Static solution

As with the discrete approach, the static equilibrium equation of the global system is written as follows:

$$EIu_h^{(4)} + k\,(x)\,u_h = F\ \delta(x - D) \tag{19}$$

$k(x)$ is the microscopic stiffness function of the node positions. To be on the macroscopic scale, it is best to calculate the limit of expressions which are functions of h ($u_h^{(4)}$, u_h) in Equation (19) when $h \to 0$. So, to resolve the 4^{th} order differential equation (19) and to calculate these limits, let us consider the vector $V = \left[u\ u^{'}\ u^{''}\ u^{'''}\right]^T$.

By replacing the derivative of V in Equation (19), the 4^{th} order differential equation is transformed into a 1^{st} order differential equation:

$$V^{'} = M\,(x)\,V\ +\ \overline{e}\ \ \in\ \ \Re^4 \tag{20}$$

$M\,(x)$ and $\overline{e}$ are the stiffness matrix and the vector related to the load F respectively.

$$M\,(x) = \begin{bmatrix} 0 & 1 & 0 & 0 \\ 0 & 0 & 1 & 0 \\ 0 & 0 & 0 & 1 \\ -\overline{k}\,(x) & 0 & 0 & 0 \end{bmatrix} \quad \text{and} \quad \overline{e}\ = \frac{F}{EI}\ \ [\ 0\ \ 0\ \ 0\ \ \delta\,(x - D)\ ]^T$$

Where $\overline{k}\,(x)$ is the microscopic stiffness and is equal to $\dfrac{1}{EI}\sum_{i=1}^{N} h\,k_i\ \delta\,(x - x_i)$. The general solution $V(x)$ of the 1^{st} order differential equation established in Equation (20) is formulated as follows:

$$V(x) = \exp\left[\int_0^x M(s)ds\right]\ \alpha(x) \tag{21}$$

The derivative of $V(x)$ in Equation (21) is written as follows:

$$\frac{dV}{dx} = \exp\left[\int_0^x M(s)ds\right]\ \alpha^{'}(x) + M(x)\,V(x) \tag{22}$$

By identifying $V'(x)$ in Equations (20) and (22), we obtain the expression of $\alpha^{'}(x)$. By applying the integral operation on $\alpha^{'}(x)$, the function $\alpha(x)$ is written as follows:

$$\alpha(x) = \alpha_0 + \int_0^x \exp\left(-\int_0^y M(s)ds\right)dy\ \ \overline{e} \tag{23}$$

The integral $\int_0^x M(s)ds$ is approximately equal to $x \prec M \succ$, where $\prec M \succ = \frac{1}{x}\int_0^x M(s)ds$ is the average of the matrix M on the interval $[0\ \ x]$. Finally by introducing the value of $\alpha(x)$ in Equation (21), the general solution of the 1^{st} order differential equation $V(x)$ becomes:

$$V(x) \approx \exp(x \prec M \succ)\,\alpha_0 + \prec M \succ^{-1}(\exp(x \prec M \succ) - 1)\ \ \overline{e} \tag{24}$$

An identification regarding the derivative of $V(x)$ calculated in the Equation (24); ($V^{'}(x) = \prec M \succ\ V + \overline{e}$) and Equation (20) shows that the general solution $V(x)$ does not change if we replace $M(x)$ by its average $\prec M \succ$ on the interval $[x - dx\,;\, x + dx]$. So the macroscopic stiffness is given by $\overline{K}(x) = \prec \overline{k}(x) \succ = \frac{1}{2dx}\int_{x-dx}^{x+dx} \overline{k}(x)dx$.

Considering the above remarks, if we replace the microscopic stiffnesses k_i by its local average in a defined interval (see Figure 6), we prove that the solution of the macroscopic approach is close to the solution of the discrete approach.

Figure 6 is approximately here

The final form of the static differential equation is given as follows:

$$u^{(4)}(x) + \overline{K}(x)\, u(x) - \frac{1}{E\, I} F\, \delta(x - D) = 0 \tag{25}$$

For the segments where $\overline{K}(x) =\prec \overline{k}(x) \succ$ is constant, the general solution of Equation (25) takes an exponential form:

$$u\,(x) = e^{(\mu\, x)}\left[\alpha \cos{(\mu\, x)} + \beta \sin{(\mu\, x)}\right] + e^{(-\mu\, x)}\left[\gamma \cos{(\mu\, x)} + \delta \sin{(\mu\, x)}\right] \tag{26}$$

α, β, γ, δ are the numerical parameters that must be calculated at each element in order to find the deflection of the macroscopic approach and $\mu = \left(\frac{\overline{K}}{4}\right)^{\frac{1}{4}}$.
We use the same formulation of parameters as with the dynamic case of the discrete approach, but it has a different solution for the differential equation. By considering the same relation established in Equation (14), the matrix R_1 becomes:

$$\tilde{R_1} = \begin{bmatrix} 1 & 0 & 1 & 0 \\ \mu_0 & \mu_0 & -\mu_0 & \mu_0 \\ 0 & -2{\mu_0}^2\, EI & 0 & 2{\mu_0}^2\, EI \\ 2{\mu_0}^3\, EI & -2{\mu_0}^3\, EI & -2{\mu_0}^3\, EI & -2{\mu_0}^3\, EI \end{bmatrix} \tag{27}$$

The relation established between Equation (15) and Equation (18) remain valid with the only changes in the form of the matrices R_2, R_3 and R_4. The new form of the matrix R_4 is written:

$$\tilde{R}_4 = \begin{bmatrix} ab & ac & bd & dc \\ \mu_0\,(ab-ac) & \mu_0\,(ac+ab) & -\mu_0\,(db+cd) & \mu_0\,(db-cd) \\ 2{\mu_0}^2\,EI\,ac & -2{\mu_0}^2\,EI\,ab & -2{\mu_0}^2\,EI\,cd & 2{\mu_0}^2\,EI\,bd \\ 2{\mu_0}^3 EI\,(ac+ab) & 2{\mu_0}^3 EI\,(ac-ab) & 2{\mu_0}^3 EI\,(cd-db) & -2{\mu_0}^3 EI\,(db+cd) \end{bmatrix}$$

Where $a = \exp(\mu_0\, L_0)$, $b = \cos(\mu_0\, L_0)$, $c = \sin(\mu_0\, L_0)$ and
$d = \exp(-\mu_0\, L_0)$.
The matrices $\tilde{R}_2$ and $\tilde{R}_3$ take the same form as the matrix $\tilde{R}_4$ by replacing the term L_0 for the variables a, b, c and d, with the term Y.

2.2.2. Dynamic solution

The resolution of the macroscopic problem in the harmonic dynamic case does not change significantly when compared to the dynamic case of the discrete approach. Changes will take place at the level of the rigidity matrix, especially in the value of the stiffness. The dynamic equlibrium equation is written as follows:

$$EI\, u_h^{(4)} + K(x)\, u_h - \rho\omega^2 S u_h = F\ \delta(x-D) \tag{28}$$

The characteristic polynomial of the differential equation is written:

$$\zeta^4 + \frac{K - \rho\omega^2 S}{E\, I} = 0 \tag{29}$$

Equation (29) possesses four complex roots; $\zeta_j = \alpha_j + i\beta_j$ where α_j and β_j represent the attenuation and the propagation waves respectively. The semi analytical solution of the differential equation in Equation (28) has the following form:

$$u(x) = A\,e^{\zeta x} + B\,e^{-\zeta x} + C\,e^{i\zeta x} + D\,e^{-i\zeta x} \tag{30}$$

ζ is the new form of the wavenumber; it is a function of the average of the discret stiffness K and the frequency of the wave: $\zeta = \left(\frac{-K + \rho\omega^2 S}{E\,I}\right)^{\frac{1}{4}}$. The relation of Equations (14) through (18) established in the dynamic case of the discrete approach are still valid. The only change is for the value of ζ where the stiffness of a spring "k" is replaced by the average of homogeneous stiffness "K".

3. Coupling approach

It is expected that there will be a difference between the behavior of beam models using the discrete approach and the macroscopic approach. Those using for both dynamic and static cases. This difference is proved later in the section by the numerical results. For these, a coupling method between these approaches which enables us to reproduce similar behavior for both discrete and coupled approach is recommended. This coupling formulation must take into account several factors: the accurate reproduction of the behavior of the system, the reduction of the number of DoF and the computation time. Moreover, in the dynamic case, the problem of possible reflection of waves at the interface of the coupling domains must be considered.

3.1. Numerical tools for the coupling approach

Let us consider an element of the beam composed of two nodes modelled by the macroscopic approach. Its equivalent in the discrete approach depends

eventually on the ratio between the size of the discrete and macroscopic elements. Initially, we calculate all the nodal parameters using the macroscopic approach. For the element of the beam under consideration, we take the values of the forces on both end nodes, insert these values in the discrete approach, and then run the calculation.

$$\begin{cases} T_d^j = T_m^i \quad \text{and} \quad T_d^{j-4} = T_m^{i-1} \\ M_d^j = M_m^i \quad \text{and} \quad M_d^{j-4} = M_m^{i-1} \end{cases} \tag{31}$$

i and j represent the number of a macroscopic node and its discrete equivalentrespectively as shown in Figure 7. T_d^i and T_m^j are the discrete and macroscopic forces at the ith and jth nodes respectively.

Figure 7 is approximately here

Thanks to this easy way, we are able to calculate the values of the nodal parameters in the discrete approach, for both ends of the considered beam element. The absolute error for the deflection and the rotation is calculated for the beam element $[\,(n - ratio)\ ,\ n\,]$ by taking the difference between the exact calculation using the macroscopic approach called U_h and the discrete approximated from macroscopic data using the discrete approach called $\tilde{U}_d$. This error is a function of the DE/ME ratio. The error function is formulated as follows:

$$e = \frac{\sum_{i=1}^{2} \left| U_h^i - \tilde{U}_d^i \right|}{\sum_{i=1}^{2} |U_h^i|} \tag{32}$$

U_h is the displacement vector calculated using the macroscopic approach; it is written: $U_h = [u_h\ \theta_h]^T$ and $\tilde{U}_d$ is the displacement vector calculated

using the discrete approach written: $\tilde{U}_d = [\tilde{u}_d \tilde{\theta}_d]^T$. DE and ME are the abbreviations of Discrete and Macroscopic Element respectively.
This criterion which is used as a numerical tool is necessary for the choice of the appropriate approach in each element.

3.2. Algorithm of resolution

Regardless of the problem to be treated, the first stage of the coupling approach consists of a discrete description of the problem. From the discrete modelling, we deduce the macroscopic approach at the coarse scale. The choice of the ratio between the size of the DE and ME is based on the close reproduction of the behavior by the macroscopic approach. Once this ratio is fixed, the macroscopic approach becomes the reference for the coupling approach. Firstly, the mechanical parameters on the first element are calculated by applying a criterion of coupling. This criterion can be summarized as follows: If the deflection and rotation errors between the discrete and macroscopic approaches are lower than 10%, the scale of computation is not changed, but if this error is higher than 10%, the discretization is refined, ie a decrease in the size of the macroscopic element. This procedure of refinement is used as long as is necessary in order to be placed on the scale of the discrete elements. In what follows, the numerical algorithm for the coupling approach is presented.

Figure 8 is approximately here

The objective of this algorithm is to produce an approach which combines between an approach on the macroscopic scale and another one on the microscopic scale. The first approach is used to model the regular zones,

the second one will be used in zones where some irregularities can occur (for example, large variation of the spring stiffnesses).

4. Numerical Results

4.1. Comparison between the Discrete and Macroscopic approaches

We implemented these approaches and elaborated several test benches in static and dynamic cases in a MATLAB code. We tested many situations of heterogeneous, homogeneous, or oscillating stiffnesses. In the case of heterogeneities under the railways, it is clear that the two approaches lead to different behavior, especially when the ratio between the number of discrete and macroscopic elements increases. This difference is illustrated more particularly in zones with heterogeneities.

In this section, we develop test cases and illustrate the difference in the behavior between these approaches. Table 1 shows the value of parameters needed in the numerical computation.

Table 1 is approximately here

4.1.1. Numerical validation of the Discrete and Macroscopic approaches

Two numerical tests are carried out to ensure the consistency of the proposed model. In the static case, we consider a beam with length L, fixed at one of its extremities, and with a load F is applied to its other one. By calculating this structure, the analytical deflection is obtained as follows:

$$U_{\text{analytical}} = \frac{F}{6EI}\, x^2\ (3L - x) \tag{33}$$

In the dynamic case, we consider the same beam, but we apply the load at the mid point of the beam. This beam is fixed at both ends. The analytical

solution has the same form as Equation (13). So to evaluate the solution we have to calculate the vector of constants $[A\,B\,C\,D]$. It is calculated by using the following equality:

$$\begin{bmatrix} A \\ B \\ C \\ D \end{bmatrix} = \begin{bmatrix} \alpha & \beta & -\alpha_c & -\beta_c \\ -\zeta\,\delta & \zeta\,\alpha & \zeta\,\delta_c & -\zeta\,\alpha_c \\ \zeta^2\,EI\,\gamma & \zeta^2\,EI\,\delta & -\zeta^2\,EI\,\gamma_c & -\zeta^2\,EI\,\delta_c \\ -\zeta^3\,EI\,\beta & \zeta^3\,EI\,\gamma & \zeta^3\,EI\,\beta_c & -\zeta^3\,EI\,\gamma_c \end{bmatrix}^{-1} \begin{bmatrix} 0 \\ 0 \\ 0 \\ F \end{bmatrix} \tag{34}$$

Where c is the point of the load,

$\alpha = cos(\zeta\,c) - cosh(\zeta\,c), \quad \alpha_c = cos\,(\zeta\,(c-L)) - cosh\,(\zeta\,(c-L)),$

$\beta = sin(\zeta\,c) - sinh(\zeta\,c), \quad \beta_c = sin\,(\zeta\,(c-L)) - sinh\,(\zeta\,(c-L)),$

$\gamma = cos(\zeta\,c) + cosh(\zeta\,c), \quad \gamma_c = cos\,(\zeta\,(c-L)) + cosh\,(\zeta\,(c-L)),$

$\delta = sin(\zeta\,c) + sinh(\zeta\,c)$ and $\delta_c = sin\,(\zeta\,(c-L)) + sinh\,(\zeta\,(c-L)).$

In this example, the discrete and macroscopic stiffnesses are equal 0 and the boundary conditions are represented by the blocking of the rotation and the deflection at the first node. In Figure 9, a perfect match is observed. In Figure 9(b), we can see the influence of the damping of Young's modulus and the stiffness of the springs on the amplitude of the wave.

Figure 9 is approximately here

4.1.2. Cases of good matching between the two approaches

Homogeneous stiffness; low and high values

In this first type of test, we examined 2 subcases:

• Low value of stiffness: Its value is considered 100 times smaller than its real value (Boussinesq solution (Ricci et al, 2006)). The deflection and the rotation at the two ends of the beam are blocked.

• High value of stiffness: Its value is the same as the value of the Boussinesq solution (Ricci et al, 2006). Similar to the preceding test, the deflection and the rotation at the two ends of the beam are blocked.

Figure 10 is approximately here

In these subcases, there is always a perfect match between the macroscopic and discrete approaches for all node parameters (deflection, rotation, bending moment and constraints in spring) as we can see in the tables of Figure 10 for the static and dynamic cases. This good match is not valid for the shear forces due to the discontinuity at the third derivative of the deflection $u(x)$.

In the case of high values for stiffness, the deflection takes a sharp form as shown in Figure 10(a) and the affected zone is near the applied load F. In the case of lower values for stiffness, Figure 10(b) shows that the affected zone is very large compared to that obtained in the case of high values stiffness.

4.1.3. Cases of significant difference between approaches

Stiffness with an area of weakness around the applied load

In this case, an area of stiffness with low values around the applied load F is considered. Furthermore the stiffness is assumed homogenous with high values. In situ, the zone of weakness can exist due to an absence or bad

distribution of the ballast under the tie track, or due to a worn tie track. Several positions of the load F are also tested.

Figure 11 is approximately here

Figure 11(a) shows the difference from the deflection of the beam in the static case. Figure 11(b) shows the variation of the error between different parameters calculated using macroscopic and discrete approaches. For example, the error on the deflection is evaluated as follows:

$$e = \frac{\sum_{i=1}^{N} \left| {u_i}^d - {u_i}^h \right|}{\sum_{i=1}^{N} \left| {u_i}^d \right|} \tag{35}$$

u^h and u^d are the macroscopic and discrete deflection respectively.
We also tested the influence of the size of the zone of heterogeneity on the behavior of the ballast studied via discrete and macroscopic approaches. When the ratio between the number of DE and ME was increasing, the weakness zone was fixed just at the point of load, the difference between the approaches becomes significant. However, when the size of the weakness zone around the applied load was increasing, the difference decreased substantially as shown in Figure 11(b). We can obtain a good agreement when the size of the weakness zone becomes significant compared to the length of the beam studied.

Oscillating stiffness

In this case, the stiffness is considered an oscillating function, as written in Equation (36):

$$K_i = \left(\cos\left(\frac{2\pi\, ih}{3}\right) + 1\right) 10^5 + 10^3 \quad (\mathrm{N.m^{-1}}) \tag{36}$$

This oscillating function has a period of 3. Firstly, tests are done by considering the same number of DoF in the two approaches and by supposing that the macroscopic stiffness oscillates identically to the microscopic stiffness.

A good match between all node parameters is shown in Figure 12(a). However by increasing the value of the DE/ME ratio, we can conclude a difference as shown in Figure 12(b) where this ratio increases progressively.

Figure 12 is approximately here

4.1.4. Error evolution for the criterion of the coupling method

Figure 13 shows the evolution of the error of the deflection and rotation of the beam element considered in section 3.1 which is necessary for the numerical criterion of the coupling apporach.

Figure 13 is approximately here

4.2. Numerical validation of the coupling approach

4.2.1. Test benches

Based on the algorithm of resolution, we implement the static and the harmonic dynamic studies of the coupling approach in a MATLAB code. In this section we present some cases studied. A comparison between discrete and coupling solution is always done in order to prove the efficiency of the coupling approach. We study the cases where the macroscopic approach cannot reproduce the same behavior as the discrete one.

4.2.2. Validation example

Firstly a sample test is done to validate the numerical implementation of the coupling approach. We consider the example dealt with section 4.1.3, the case where we have a homogeneous stiffness with a zone of heterogeneity at the point of load.

Figure 14 is approximately here

In this example we implement the coupling approach where we use the discrete approach in the zone of heterogeneity $(45 \div 55\,m)$ and further we use the macroscopic approach. The size of the discrete zone is between $(40\,,\,60\,m)$. A good match between the coupling and the discrete behaviors is shown in Figure 14.

4.2.3. Stiffness with a zone of heterogeneity around the applied load

This proposed test is very close to reality. This situation often occurs when a tie is either broken or moved under the railway, as well as when a vacuum is created under a tie. Numerically, these real problems are replaced by heterogeneities in the stiffnesses of the springs which replace the ties and the grains of ballast. In the previous comparison, we concluded on a perceptible difference between the discrete behavior and the macroscopic one. It is proposed to study this case via the coupling approach.

Figure 15 is approximately here

In the numerical computation, we conclude that the coupling approach is able to detect the place of these heterogeneities. In this case, a refinement of the scale of computation is also observed at these heterogeneities as we

can see in Figure 15(b). Indeed, in the example simulated in Figure 15(b), we have employed some local heterogeneties where the stiffness is considered to be between 10 and 30 times less than that of the rest of the beam. The coupling approach has succesfully detected their locations. In Figure 15(a), a good match between the discrete deflection and the coupling one in the dynamic case is observed. This result is similar to that of the static case.

4.2.4. Stiffness with arbitrary values

In this case, we consider the stiffness of the discrete approach to be an arbitrary function which varies between two values ($k_{\min}$ and $k_{\max}$).

$$k_i = (k_{\max} - k_{\min}) \times rand(n, 1) + k_{\min} \tag{37}$$

The macroscopic stiffness is the average of the local microscopic stiffnesses as proved in section 2.2.1. By comparing the discrete and the macroscopic solution in the static and dynamic cases, we have observed a difference between the different node parameters. Then, the coupling approach is employed to make a better simulation than the macrosopic one. Figure 16 shows the good matching between the discrete and coupling solutions.

Figure 16 is approximately here

It should be noted that the coupling approach is applied in the case of homogeneous stiffnesses. In the comparison of the discrete and macroscopic solutions, it is concluded that the macroscopic approach adequatly replaces the discrete one. Once this coupling approach is applied, we find that no refinement of the macroscopic scale computation is needed.

4.2.5. Error evolution

Here, we consider the example dealt within section 4.2.3. We calculate the error at each node between the discrete and the coupled deflection and rotation. At the first iteration, this error is maximized, because the coupling approach still the same as the macroscopic with coarse element. While increasing the iteration number, we can observe that this error decreases substantially. Figure 17 shows the evolution of the deflection and rotation errors in the static case. In the dynamic case, the evolution of the deflection and rotation errors is similar to that of the static case.

Figure 17 is approximately here

4.2.6. Spurious wave reflection

An obvious challenge that arises from the problem of coupling between fine and coarse scales, is that of the reflexion of the wave at the coupling interface. For the correct propagation and representation of a wave in an element, it is necessary that its wavelength be at least 5 times larger than the size of this element. Then, if a wave carries out a brutal passage from a fine scale to a coarse one, the problem of the reflexion wave must be taken into account. In our case, the coupled approach is at its base a macroscopic approach with coarse elements. Thus, the propagation of a wave through the elements of this mesh means that its wavelength is adapted to this type of mesh. When its obliged to become refined in mesh, the wave will not have a problem to continuing to propagate in the new mesh, because the wavelength in this case is represented by a number of elements higher than that of the starting discretization.

In conclusion, the reflexion of the wave of scale variations between coarse-fine is not a problem in this study. If a problem of reflexion arises, it means that from the begining the wavelength is not adapted to the mesh and the problem does not come from the coupling scale. The absence of spurious waves in the coupling approach is viewed as an advantage.

4.2.7. Gain in the number of DoF

In this section, we elaborate the same test benches elaborated in section 4.1.1. In all these tests, the starting approach is macroscopic with coarse elements. A comparison between discrete and coupling approaches is always done. The objective of this approach is to reproduce accurately the behavior of the structure while decreasing the degrees of freedom (DoF) and the computing time. A good match between the mechanical parameters is obtained. In each test, the ratio between the number of CE (Coupling Element) and DE (Discrete Element) is calculated. Table 2 shows the evolution of this important factor. It also shows that the value of this gain ratio is oscillating between 2 and 3.

Table 2 approximately is here

Heterogeneity and **r** mean the test case where we have hetreogeneity in the stiffness and the ratio between DE and ME numbers respectively.

5. Extension to 2D problems

After validation of our proposed coupling method on the 1D railway model, an extension to a 2D problem is in progress. We study a 2D model which

consists of a regular lattice of square rigid grains interacting by their elastic interfaces (see figure 18).

Figure 18 is approximately here

Two models have been developed, a discrete one and a continuous one. In the discrete model, the grains which form the lattice are modeled as rigid bodies connected by elastic interfaces (elastic thin joints). In other words, the lattice is seen as a "skeleton" in which the interactions between the rigid grains are represented by forces and moments which depend on their relative displacements and rotations. The continuous model is based on the homogenization of the discrete model (Cecchi & Sab (2009), Cecchi & Sab (2006)). Considering the case of singularities within the lattice (a crack for example), we will develop a coupling model which uses the discrete model in singular zones (zones where the discrete model cannot be homogenized), and the continuous model elsewhere. Here a brief description of the coupling model is presented.

5.1. Principle of the coupling method

The medium is decomposed in two regions. The first one is the continuum region modeled by finite elements (rectangular with 2 DoFs by node), the second is the discrete region where the DE are the centre of grains (3 DoFs at the center of grains). At the interface between these zones, interpolated DE are used to link the FE of the continuum zone to the DE of the discrete zone (see figure 19).

Figure 19 is approximately here

Noting $\mathbf{E}^{\text{discrete}}$ the elastic energy of the discrete zone, $\mathbf{E}^{\text{continuum}}$ the elastic energy of the continuum zone and $\mathbf{E}^{\text{interaction}}$ the energy of the interaction between the DE and the FE, the total energy of the coupled medium is written :

$$\mathbf{E}^{\text{total}} = \mathbf{E}^{\text{discrete}} + \mathbf{E}^{\text{continuum}} + \mathbf{E}^{\text{interaction}} \tag{38}$$

The interaction energy between two DEs (- and +) is written as follows :

$$\mathbf{E}^{\text{interaction}} = \frac{1}{2} \begin{pmatrix} \mathbf{U}^- \\ \mathbf{U}^+ \end{pmatrix}^{\text{T}} \left[\mathbf{K}^{\text{interface}}\right] \begin{pmatrix} \mathbf{U}^- \\ \mathbf{U}^+ \end{pmatrix} \tag{39}$$

$\mathbf{K}^{\text{interface}}$ is the stiffness matrix of the interface between two adjacents grains. $\mathbf{U}^-$ and $\mathbf{U}^+$ are the vectors of displacements and rotation of the grains (-) and (+), respectively.

If we consider a FE modeled by DEs, a relationship between the displacement of the FE node's ($\square$) and the displacement of the DE ($\circ$ created inside the FE) can be established by interpolation, using the shape functions. By noting $[U\,,V\,,W]^T$ the vector of displacement and rotation of a DE and $[u_1\,,v_1\,,u_2\,,v_2\,,u_3\,,v_3\,,u_4\,,v_4]^T$ the vector of nodal displacement of a FE, the relationship writes :

$$\left[\ U\,,V\,,W\ \right]^T = \underline{\underline{\mathbf{D}}}\ \left[\ u_1\,,v_1\,,u_2\,,v_2\,,u_3\,,v_3\,,u_4\,,v_4\ \right]^T \tag{40}$$

$\underline{\underline{\mathbf{D}}}$ is a interpolation matrix.

At the same time, each DE located at the edge of the discrete zone (B^D) is connected to an interpolated DE located at the edge of the continuum zone (B^C) by adding half of the interaction energy (39) to the total elastic energy.

Thus, from these two relationships, a DE located in the discrete zone is linked to a FE in the continuum zone. If we use equation (40) for the interpolated DE ($\mathbf{U}^-$ or $\mathbf{U}^+$), then the interaction energy (39) between the DE and the FE will be a quadratic function of $\mathbf{U}^{\mathrm{D}}$ and $\mathbf{U}^{\mathrm{C}}$.
$\mathbf{U}^{\mathrm{D}}$ and $\mathbf{U}^{\mathrm{C}}$ are the global displacements vector of the discrete and continuum zones respectively. By designing $\mathbf{K}^{\mathrm{D}}$ and $\mathbf{K}^{\mathrm{C}}$ the discrete and continuum stiffness matrices, the total energy of the medium will be :

$$\mathbf{E}^{\mathrm{total}} = \frac{1}{2} \begin{pmatrix} \mathrm{U}^{\mathrm{C}} \\ \mathrm{U}^{\mathrm{D}} \end{pmatrix}^{\mathrm{T}} \underbrace{\left[\left(\begin{array}{c|c} \mathbf{K}^{\mathrm{C}} & 0 \\ \hline 0 & \mathbf{K}^{\mathrm{D}} \end{array} \right) + \left(\mathbf{K}^{\text{C-D}}\right) \right]}_{\mathbf{K}^{\mathrm{global}}} \begin{pmatrix} \mathrm{U}^{\mathrm{C}} \\ \mathrm{U}^{\mathrm{D}} \end{pmatrix} \tag{41}$$

$\mathbf{K}^{\text{C-D}}$ is the global matrix of interaction which is calculated by the summation of all elementary interaction energies between DE and FE.
As like as for the 1D methodolgy, a criterion of coupling is developed to limit the size of the discrete zone used in the singular zone. The idea is to apply discrete external forces and moments on the DE located at the edege of a FE near the interface zone and to compare the discrete responses of the grains inside the FE to their interpolated FE responses.

Figure 20 is approximately here

The external loading is computed as follows: Using equation (40), the displacements at the center of the interpolated DE created in the FE can be calculated. From the interaction energy formulated in (39), we calculate the interaction forces and moment between these 2 DE using the relation ($\mathbf{F} = \left[\mathbf{K}^{\mathrm{interface}}\right] . \left[\mathbf{U}^+ , \mathbf{U}^-\right]^T$). All the interaction forces between a DE ($\bullet$) and an external interpolated DE ($\circ$) at the edge of FE are computed and

assembled to form the external global load applied on the discrete zone included in the FE.

Using the discrete model, we calculate the discrete displacements of the DE noted as $\mathbf{U}^{\text{discrete}}_{\text{approximated}}$. After that, we calculate the difference between the interpolated continuum displacements in equation (40) ($\mathbf{U}^{\text{continuum}}_{\text{interepolated}}$) at the center of grains and $\mathbf{U}^{\text{discrete}}_{\text{approximated}}$. This difference will be the criterion for coupling. It is formulated as follows :

$$\text{error} = \left| \frac{\mathbf{U}^{\text{discrete}}_{\text{approximated}} - \mathbf{U}^{\text{continuum}}_{\text{interpolated}}}{\mathbf{U}^{\text{discrete}}_{\text{approximated}}} \right| \tag{42}$$

If this error is more than 10%, the scale of computation will be that of the discrete model. In the other case, the continuum scale of computation is adapted. Due to this criterion, the size of the discrete region is controled and the number of DoF is reduced.

More details of discrete and continuum models will be the object of a future publication.

6. Conclusion

In this paper, we presented a formulation used for coupling discrete and continuum mediums. This coupling approach can be used to study models which represent some irregularities (heterogeneity, crack and so on). For a direct application of this approach, we considered a beam resting on tie tracks and on grains of ballast modelled by springs with elastic behavior. This model is studied in both dynamic and static cases. First, this model is calculated via discrete and macroscopic approaches. We proved the existence of several cases where the macroscopic approach cannot replace

the discrete one. Due to this difference, a coupling approach between discrete and continuum ones was proposed. This approach consists of a continuum approach derived from the discrete one at macroscopic scale. The macroscopic elements have a coarse size compared to the discrete ones. Using a criterion of coupling, the size of these elements should be refined when necessary. This procedure should be repeated until the size of the ME is the same as that of a DE.

After applying the coupling approach in the cases where the macroscopic and discrete approaches do not give an identical behavior of the ballast, we could show the efficiency of this approach and summarize it in some points. Firstly, we observe a good match between the discrete and the coupling behaviors. Secondly, we observe a gain in the number of elements, which implies a reduction in the computation time compared to that needed in the discrete approach. This approach can also detect the locations of heterogeneities. In addition to these conclusions, the absence of the spurious wave at the interface of coupling is also proved. In future works, this coupling approach will be extended to 2 and 3 dimensional problems.

References

A.Al Shaer, D.Duhamel, K.Sab, G.Foret, L.Schmitt, (2008). Experimental settlement and dynamic behavior of a portion of ballasted railway track under high speed trains. Journal of Sound and Vibration, 316, p. 211-233.

A.Al Shaer, D.Duhamel, K.Sab, L.M. Cottineau, P.Hornych, L.Schmitt, (2005).Dynamical experiment and modeling of a ballasted railway track bank. EURODYN 2005: sixth European conference on structural dynamics 3, p. 2065-2070.

H.Ben Dhia, G.Rateau, (2001). Analyse mathématique de la méthode Arlequin mixte. C.R.Acad.Sci.Paris, t.332, Série, p. 649-654.

H.Ben Dhia, G.Rateau, (2005). The Arlequin method as a flexible engineering design tool. International Journal for Numerical Methods in Engineering, 62, p. 1442-1462.

V. Bodin-Bourgoin, P.Tamagny, K.Sab, PE.Gautier, (2006).Experimental determination of a settlement of the ballast portion of railway tracks subjected to lateral charging. CANADIAN GEOTECHNICAL JOURNAL 43 (10), p. 1028-1041.

J.Q. Broughton, F.F. Abraham, N. Bernstein, E. Kaxiras, (1999). Concurrent coupling of length scales: methodology and application. Physical Review B 60, p. 2391-2403.

A. Cecchi, K. Sab, (2009). Discrete and continuous models for in plane loaded random elastic brickwork. European Journal of Mechanics - A/Solids, 28, p.610 - 625

A. Cecchi, K. Sab, (2006). Corrigendum to A comparison between a 3D discrete model and two homogenised plate models for periodic elastic

brickwork [International Journal of Solids and Structures 41 (2004) 2259-2276]. International Journal of Solids and Structures, 43, p. 390-392.

P. A. Cundall, O.D.L. Stack, (1979). A discrete numerical model for granular assemblies. Geotechnique 29, 47-65.

W.A.Curtin, R.A.Miller, (2003). Atomistic/continuum coupling in computational materials science. Modelling and Simulation in Materials Science and Engineering, 11, R33-R68.

J.Fish, W.Chen, (2004). Discrete-to-continuum bridging based on multigrid principles Computer Methods in Applied Mechanics and Engineering, 193, Issues 17-20, p. 1693-1711.

E.Frangin, P.Marin, L.Daudeville, (2006). Coupled finite/discrete elements method to analyze localized impact on reinforced concrete structure. In: Proceedings EURO-C.

P.A. Klein, J.A. Zimmerman, (2006). Coupled atomistic-continuum simulations using arbitrary overlapping domains. Journal of Computational Physics 213, p. 86-116.

J.Knap, M.Ortiz, (2001). An analysis of the quasicontinuum method. Journal of the Mechanics and Physics of Solids 49, p. 1899-1923.

S.Kohlhoff, S.Schmauder, (1989). A new method for coupled elastic-atomistic modelling in: V. Vitek, D.J. Srolovitz (Eds), Atomistic Simulation of materials. In: Beyond Pair Potentials, Plenum Press, New York, pp. 411-418.

R. E.Miller, E. B.Tadmor, (2009). Topical Review : A unified framework and performance benchmark of fourteen multiscale atomistic/continuum coupling methods. Modelling and Simulation in Material Science and

Engineering, 17 (053001), 51 pp.

Vu-Hieu Nguyen, Denis Duhamel, (2006). Finite element procedures for nonlinear structures in moving coordinates. Part1: Infinite bar under moving axial loads. Computers & Structures, 84, p. 1368-1380.

Vu-Hieu Nguyen, Denis Duhamel, (2008). Finite element procedures for nonlinear structures in moving coordinates. Part II: Infinite beam under moving harmonic loads. Computers & Structures, 86, p. 2056-2063.

L. Ricci, V.H. Nguyen, K. Sab, D. Duhamel, L. Schmitt, (2005). Dynamic behaviour of ballasted railway tracks: A discrete/continuous approach. Computers & Structures, 83, Issues 28-30, p. 2282-2292.

L.Ricci, K.Sab, (2006). Influence des plates-formes sur le tassement des voies ferrées ballastées. PhD thesis, Ecole Nationale des Ponts et Chaussées.

R.E. Rudd, J.Q. Broughton, (1998). Coarse-grained molecular dynamics and the atomic limit of finite elements. Physical Review B 58, p. R5893-R5896.

V.B. Shenoy, R. Miller, E.B. Tadmor, D. Rodney, R. Philips, M. Ortiz, (1999). An adaptative finite element approach to atomic-scale mechanics - the quasicontinuum method. Journal of the Mechanics and Physics of Solids 47, p. 611-642.

E.B. Tadmor, M.Ortiz, R.Philips, (1996). Quasicontinuum analysis of defects in solids. Philosophical Magazine A 73 (6), p. 1529-1563.

G.J. Wagner, W.K. Liu, (2003). Coupling of atomistic and continuum simulations using a bridging scale decomposition. Journal of Computational Physics 190, p. 249-274.

S.P. Xiao, T. Belytschko, (2004). A bridging domain method for coupling continua with molecular dynamics. Computer Methods in Applied Mechanics and Engineering 193, p. 1645-1669.

Appendix

In the section 2.1.1, we have concluded on a relationship that gives the value of parameters $P,\ Q,\ R$ and S. Here, we develop the method which is used to prove this relationship. Using Equations (3) and (4) we conclude on the following equalities:

$$\begin{cases} U_{0^+} = T_1\ [A\ B\ C\ D]^T \\ U_{Y^-} = T_2\ [A\ B\ C\ D]^T \\ U_{Y^+} = T_3\ [P\ Q\ R\ S]^T \\ U_{h^-} = T_4\ [P\ Q\ R\ S]^T \end{cases}$$

Where

$$T_1 = T_4 = \begin{bmatrix} 0 & 0 & 0 & 1 \\ 0 & 0 & 1 & 0 \\ 0 & 1 & 0 & 0 \\ 1 & 0 & 0 & 0 \end{bmatrix}\ ;\ T_2 = \begin{bmatrix} \frac{Y^3}{6} & \frac{Y^2}{2} & Y & 1 \\ \frac{Y^2}{2} & Y & 1 & 0 \\ Y & 1 & 0 & 0 \\ 1 & 0 & 0 & 0 \end{bmatrix}$$

$$T_3 = \begin{bmatrix} \frac{(Y-h)^3}{6} & \frac{(Y-h)^2}{2} & (Y-h) & 1 \\ \frac{(Y-h)^2}{2} & (Y-h) & 1 & 0 \\ (Y-h) & 1 & 0 & 0 \\ 1 & 0 & 0 & 0 \end{bmatrix}$$

$$\begin{cases} U_{0^+} &= \left[u(0^+)\ u'(0^+)\ u''(0^+)\ u'''(0^+)\right]^T \\ U_{Y^-} &= \left[u\left(Y^-\right)\ u'\left(Y^-\right)\ u''\left(Y^-\right)\ u'''\left(Y^-\right)\right]^T \\ U_{Y^+} &= \left[u\left(Y^+\right)\ u'\left(Y^+\right)\ u''\left(Y^+\right)\ u'''\left(Y^+\right)\right]^T \\ U_{h^-} &= \left[u(h^-)\ u'(h^-)\ u''(h^-)\ u'''(h^-)\right]^T \end{cases}$$

Reminding the conditions of continuity at the point of load "Y" on u, $u^{'}$ and $u^{''}$ and the jump condition on $u^{'''}$(Equation (5)) and using the above relations, the relationship between the vectors U_{h^-} and U_{0^+} is written in the following matrix form:

$$U_{h^-} = T_4\, {T_3}^{-1}\, T_2\, {T_1}^{-1}\, U_{0^+} + T_4\, {T_3}^{-1}\, \frac{F}{EI} \tag{43}$$

Replacing the value of the matrix elements in Equation (43), we deduce the value of parameters $P,\ Q,\ R,\ S$ as written in the Equation (6).
In the section 2.1.2, we have concluded on two relationships that link U_{Y^-} to the vector g and U_{Y^+} to the vector $\tilde{g}$. They are represented in the following system:

$$\begin{cases} U_{Y^-} = R_2\, [\alpha\ \beta\ \gamma\ \delta]^T \\ U_{Y^+} = R_3\, [\tilde{\alpha}\ \tilde{\beta}\ \tilde{\gamma}\ \tilde{\delta}]^T \end{cases}$$

Where

$$R_2 = R_3 = \begin{bmatrix} a_1 & b_1 & c_1 & d_1 \\ \xi_1\, a_1 & -\xi_1\, b_1 & i\,\xi_1\, c_1 & -i\,\xi_1\, d_1 \\ -E\,I\,\xi_1^2\, a_1 & -E\,I\,\xi_1^2\, b_1 & E\,I\,\xi_1^2\, c_1 & E\,I\,\xi_1^2\, d_1 \\ -E\,I\,\xi_1^3\, a_1 & E\,I\,\xi_1^3\, b_1 & i\,E\,I\,\xi_1^3\, c_1 & -i\,E\,I\,\xi_1^3\, d_1 \end{bmatrix} \tag{44}$$

Where $a_1 = e^{\xi_1 Y}$, $b_1 = e^{-\xi_1 Y}$, $c_1 = e^{i\,\xi_1 Y}$ and $d_1 = e^{-i\,\xi_1 Y}$.
These relationships are used to prove the relation between U_h and U_0 established in equation (16).

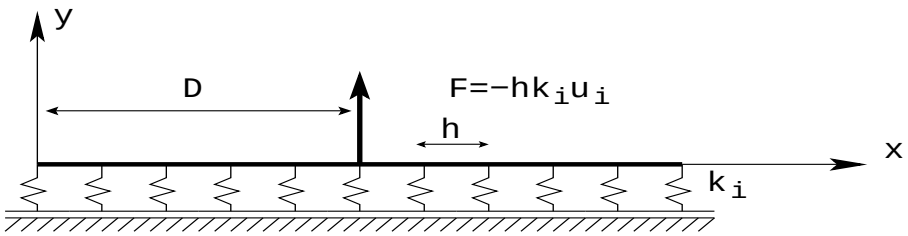

Figure 1: Proposed model (1D); Discrete modelling

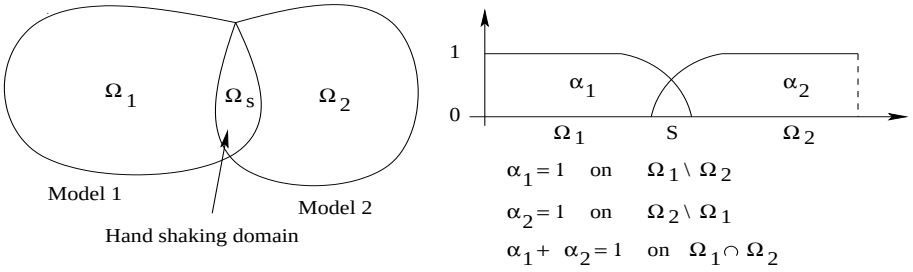

Figure 2: Arlequin method: Overlapping domains

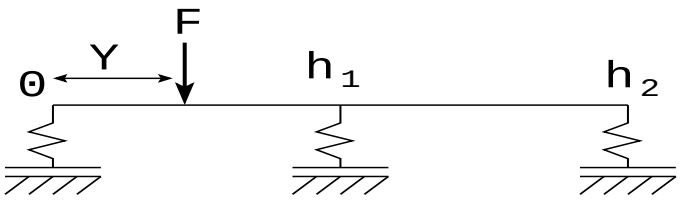

Figure 3: Two adjacent elements of beam

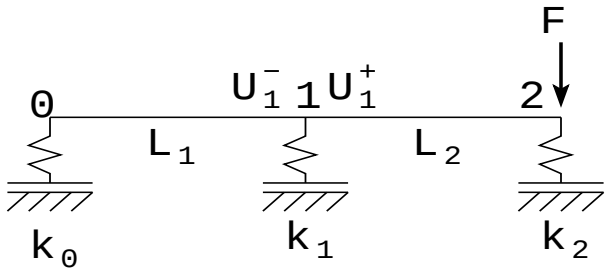

Figure 4: Conditions of continuity at node 1

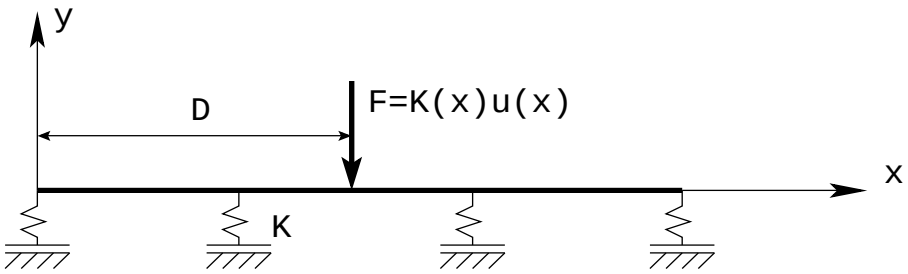

Figure 5: Macroscopic beam with the stiffness of springs

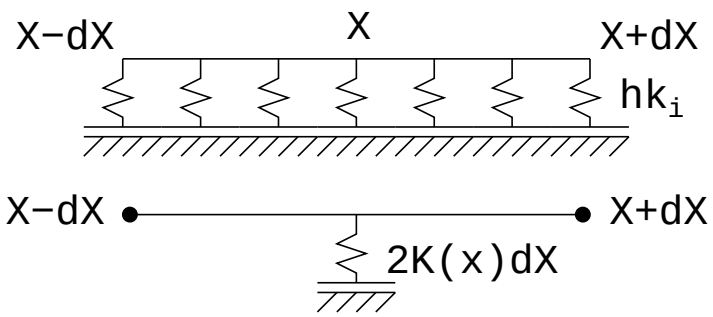

Figure 6: Relation between microscopic and macroscopic stiffnesses

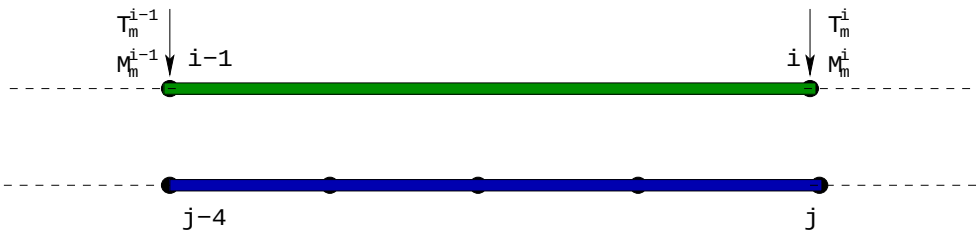

Figure 7: Beam element $[c-1\,;\,c]$ for the macroscopic approach; $[c-4\,;\,c]$ for the discrete approach. Ratio (ED/ME)=4

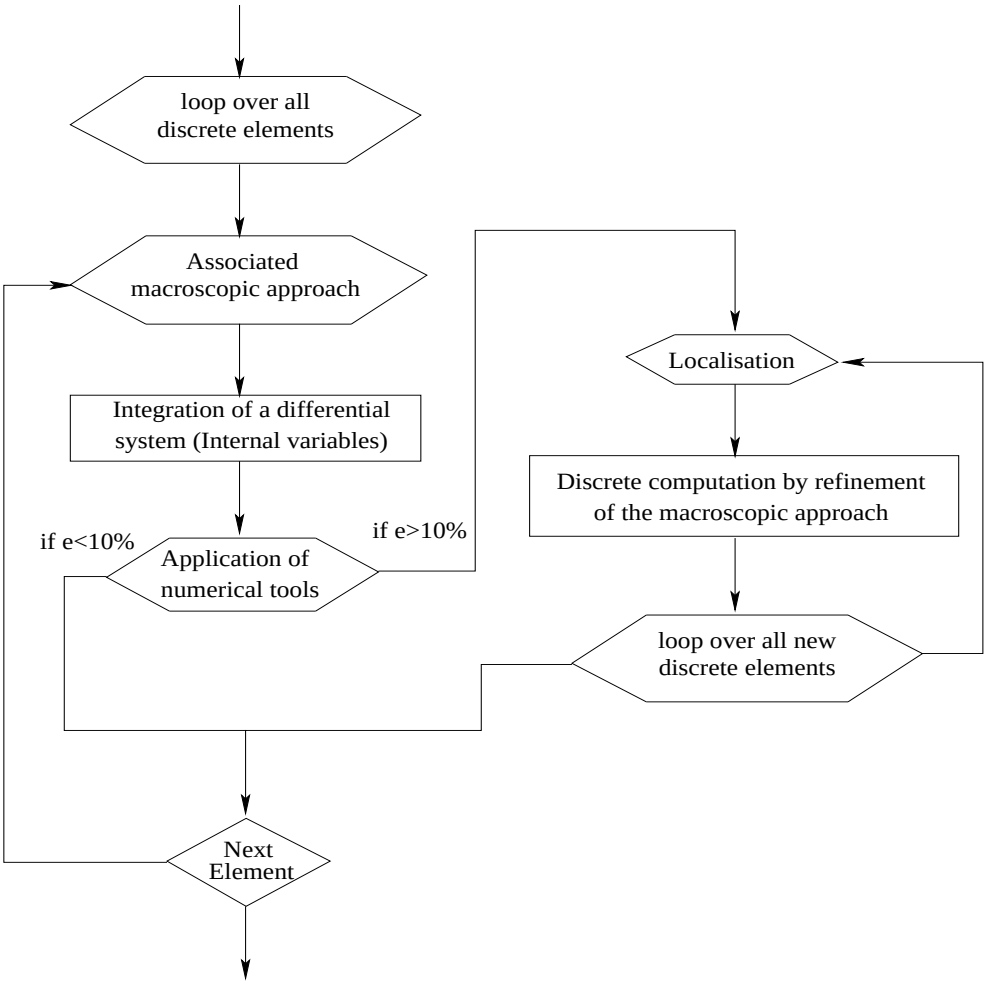

Figure 8: Numerical algorithm for the coupling approach

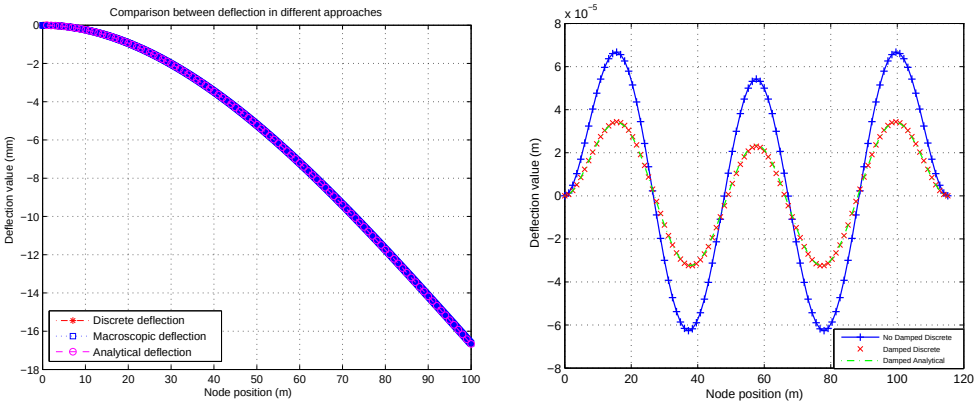

(a) (b)

Figure 9: Numerical validation of the proposed model with the analytical solution: (a) Static case ; (b) Dynamic case

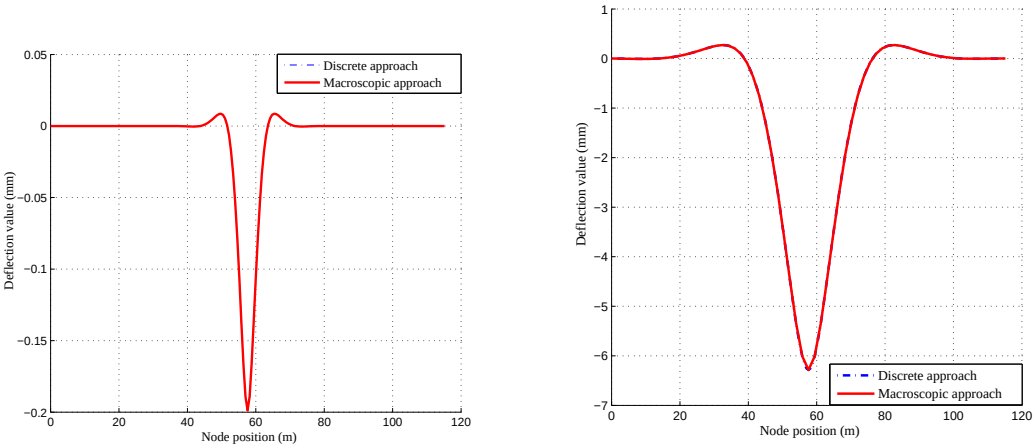

(a) (b)

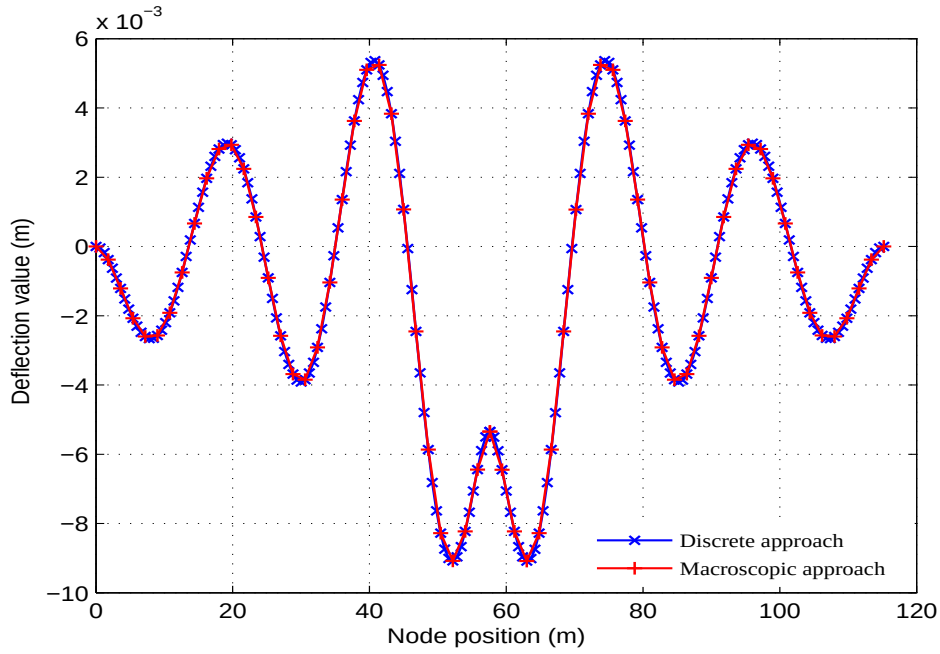

(c)

Figure 10: (a) and (b): Deflection in case of high and low stiffness values in the static case; (c): Deflection in case of low stiffness in the dynamic case

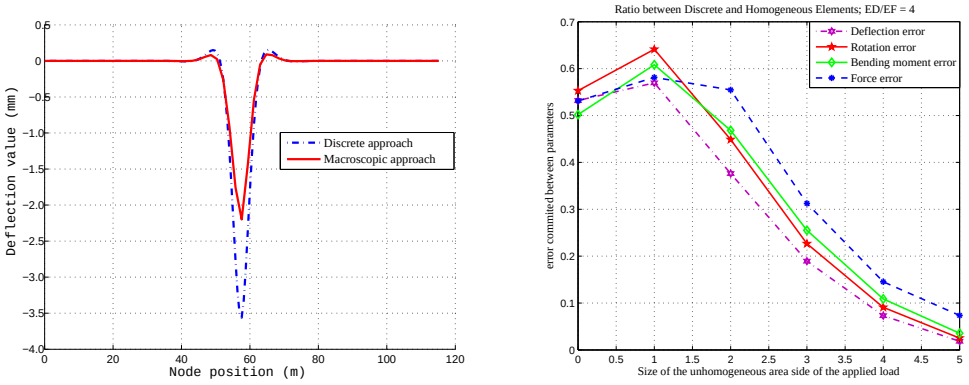

(a) (b)

Figure 11: (a) Deflection in two approaches; ratio DE/ME = 3; (b) Error evolution versus the ratio

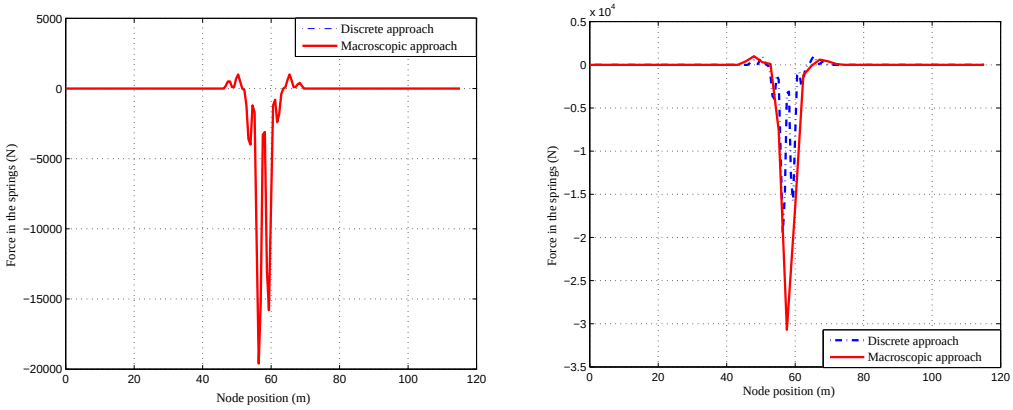

(a) (b)

Figure 12: (a) and (b) Forces in the springs; Case of oscillating stiffness; ratio = 1 and ratio = 4 respectively

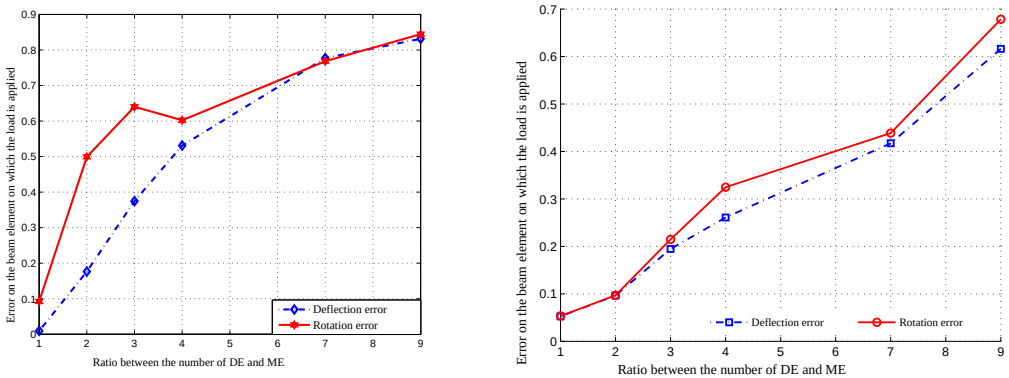

(a) (b)

Figure 13: Evolution of the deflection and rotation errors, function of the ratio between the DE and ME; (a) static case (b) dynamic case

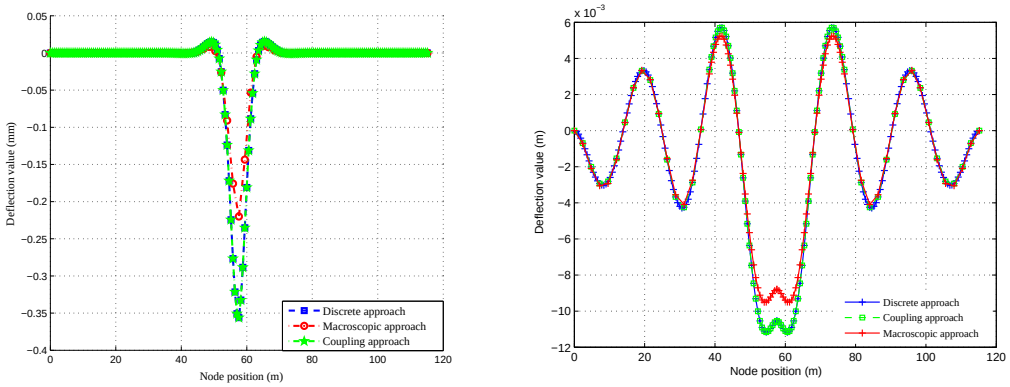

(a) (b)

Figure 14: Validation of the numerical implementation of the coupled approach; (a) static case (b) dynamic case

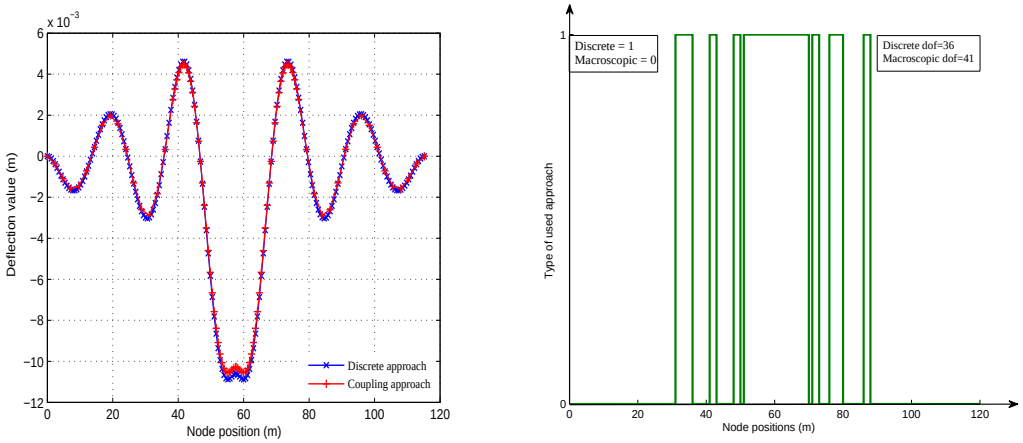

(a) (b)

Figure 15: Example of heterogeneties in the stiffnesses of the springs; (a) Deflection calculated via discrete and coupling approaches (dynamic case) (b) Type of scale used at each node in the coupled approach (static case)

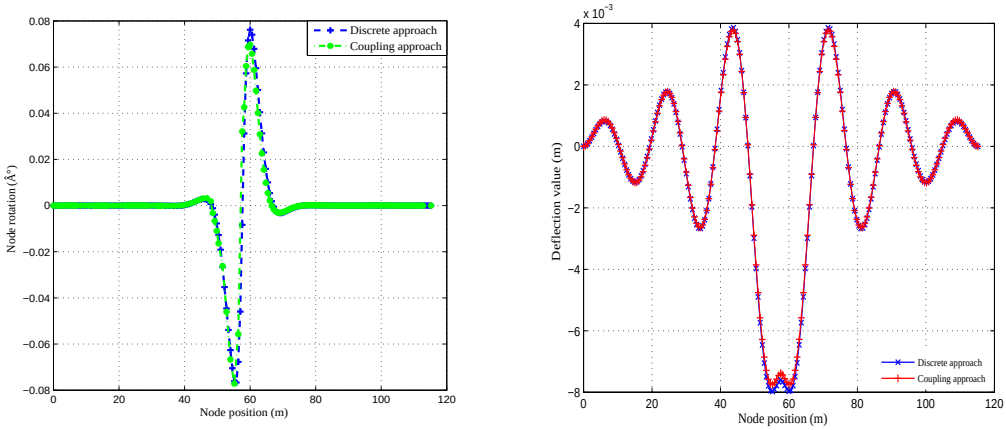

(a) (b)

Figure 16: Comparison between deflection and rotation calculated in a discrete and coupling approaches; (a) rotation in static case (b) deflection in dynamic case

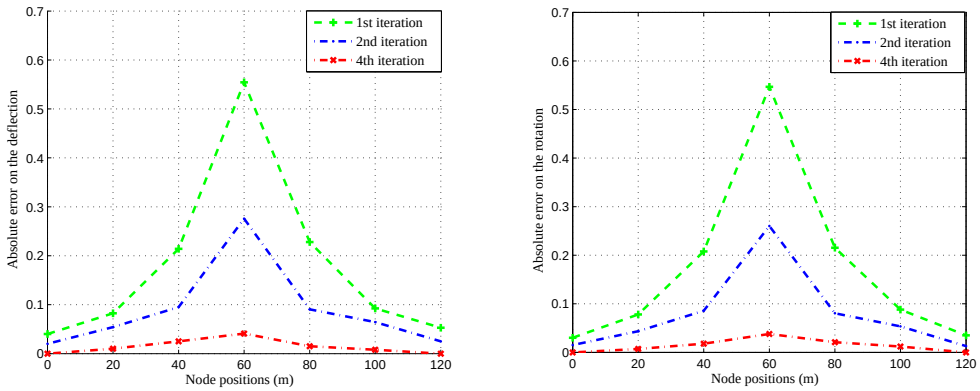

Figure 17: Evolution of the deflection and rotation errors, function of the iteration numbers; Static case

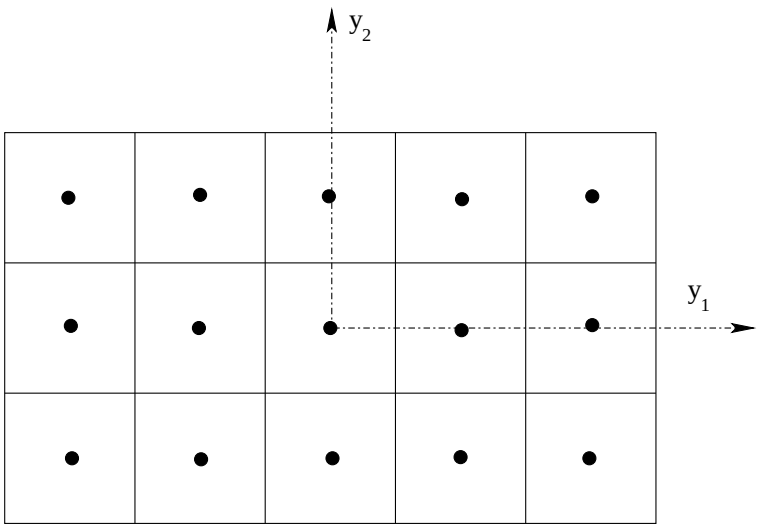

Figure 18: Square grains forming the regular lattice.

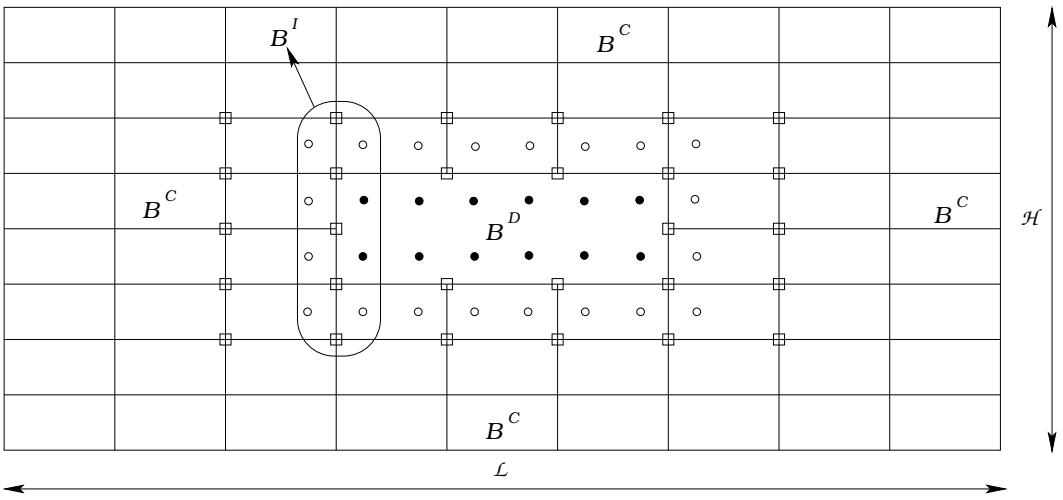

Figure 19: Regular lattice of square grains modeled by a coupling discrete/continuum model; (•) are the DE of the region (B^D), (○) are the interpolated DE of the (B^I) and (□) are the finite element nodes of the region (B^C)

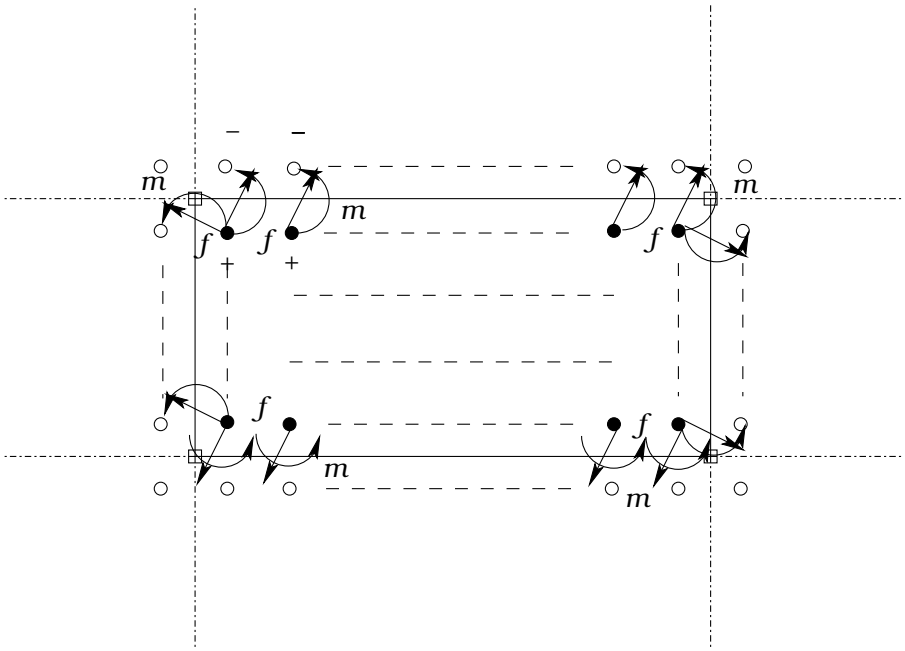

Figure 20: (f, m) are the forces and the moments of interaction between DEs inside the considered FE ($\bullet$) and interpolated DEs ($\circ$) inside adjacent FEs.

Parameters	Values	Units
Young's modulus of steel (Al Shaer et al, 2005)	$E_{\text{steel}} = 210$	GPa
Quadratic moment of a section	$I = 1,65\,.10^{-5}$	m^4
Applied load (Nguyen & Duhamel, 2008) (Al Shaer et al, 2008)	F = 80	KN
Beam length	L = 120	m
Space between tie track	h = 0.6	m
Discrete stiffness (Nguyen & Duhamel, 2006)	$k = 10^4 \div 5\,.10^5$	N/m
Macroscopic stiffness	$K = \prec k \succ$	N/m
Ratio between DE and ME numbers	R = 1, 2, 3, 4, 7, 9	
Mass per unit of surface	$\rho\, S$ = 60.3	Kg /r
Frequence of the propagating wave	$f = 0.5 \div 1$	Hz
Damping of the steel Young's modulus	$\nu = 0.05 \div 0.1$	
Damping of the spring's stiffness	$\xi = 0.1 \div 0.3$	

Table 1: Mechanical and numerical parameters used in the numerical simulations

Test cases	Dis approach	Mac approach	Coupling approach			
	DE	ME	Total	DE	ME	Gain
Heterogeneity (r=4)	**200**	50	**77**	36	41	**2.6**
Heterogeneity (r=7)	**211**	31	**73**	50	23	**2.9**
Heterogeneity (r=9)	**217**	25	**73**	54	19	**3**
Oscillating (r=4)	**200**	50	**85**	50	35	**2.4**
Oscillating (r=7)	**211**	31	**79**	57	22	**2.7**

Table 2: Influence of the coupling approach on the number of DoF